Molecular Pharmacology Fast Forward. Published on September 28, 2016 as DOI: 10.1124/mol.116.105015
This article has not been copyedited and formatted. The final version may differ from this version.

The role of the second extracellular loop of the adenosine A_1 receptor on allosteric modulator binding, signaling and cooperativity

Anh T.N. Nguyen, Elizabeth A. Vecchio, Trayder Thomas, Toan D. Nguyen, Luigi Aurelio, Peter J. Scammells, Paul J. White, Patrick M. Sexton, Karen J. Gregory, Lauren T. May, Arthur Christopoulos

Monash Institute of Pharmaceutical Sciences (A.T.N.N., E.A.V, T.T., K.J.G, L.A., P.J.S., P.J.W., P.M.S., L.T.M., A.C.), Monash e-Research Centre (T.D.N.) and Department of Pharmacology (A.T.N.N., E.A.V., K.J.G., P.M.S., L.T.M., A.C), Monash University, Victoria, Australia

Molecular Pharmacology Fast Forward. Published on September 28, 2016 as DOI: 10.1124/mol.116.105015
This article has not been copyedited and formatted. The final version may differ from this version.

Running title: Identification of the A_1AR allosteric site

Correspondence:

To whom correspondence should be addressed:

Arthur Christopoulos and Lauren T May

Drug Discovery Biology and Department of Pharmacology,

Monash Institute of Pharmaceutical Sciences,

Monash University,

399 Royal Parade, Parkville,

VIC 3052, Australia,

Tel.:(613) 9903-9095

Fax: (613) 9903-9581

E-mail: arthur.christopoulos@monash.edu, lauren.may@monash.edu

Manuscript information:

Number of text pages: 18

Number of tables: 2

Number of figures: 8

Number of references: 57

Number of words in abstract: 248

Number of words in introduction: 750

Number of words in discussion: 1502

Molecular Pharmacology Fast Forward. Published on September 28, 2016 as DOI: 10.1124/mol.116.105015
This article has not been copyedited and formatted. The final version may differ from this version.

Non-standard abbreviations

3xHA-A_1AR, human A_1AR containing an amino terminal triple human influenza hemagglutinin epitope tag; [^{3}H]DPCPX, 8-cyclopentyl-1,3-dipropylxanthine, [dipropyl-2,3-^{3}H(N)]; A_1AR, adenosine A_1 receptor; AR, adenosine receptor; ATL525, (2-amino-4,5,6,7-tetrahydro-benzo[b]thiophen-3-yl) biphenyl-4-yl-methanone); CHO, Chinese hamster ovary; ECL2, second extracellular loop; GPCR, G protein-coupled receptor; HA, human influenza hemagglutinin; MD, molecular dynamics; NECA, 5'-*N*-ethylcarboxamidoadenosine; PAM, positive allosteric modulator; PBS, phosphate buffered saline; PD81723, 2-amino-4,5-dimethyl-3-thienyl)-[3-(trifluoromethyl)phenyl]methanone; PME, particle mesh Ewald; POPC, 1-palmitoyl-2-oleoyl-sn-glycero-3-phosphocholine; TM, transmembrane; VCP171, (2-amino-4-(3-(trifluoromethyl)phenyl)thiophen-3-yl)(phenyl)methanone; WT, wild-type.

Molecular Pharmacology Fast Forward. Published on September 28, 2016 as DOI: 10.1124/mol.116.105015
This article has not been copyedited and formatted. The final version may differ from this version.

Abstract

Allosteric modulation of adenosine A_1 receptors (A_1ARs) offers a novel therapeutic approach for the treatment of numerous central and peripheral disorders. However, despite decades of research, there is a relative paucity of structural information regarding the A_1AR allosteric site and mechanisms governing cooperativity with orthosteric ligands. We combined alanine-scanning mutagenesis of the A_1AR second extracellular loop (ECL2) with radioligand binding and functional interaction assays to quantify effects on allosteric ligand affinity, cooperativity and efficacy. Docking and molecular dynamics (MD) simulations were performed using an A_1AR homology model based on an agonist-bound A_{2A}AR structure. Substitution of $E172^{ECL2}$ for alanine reduced the affinity of the allosteric modulators, PD81723 and VCP171, for the unoccupied A_1AR. Residues involved in cooperativity with the orthosteric agonist, NECA, were different between PD81723 and VCP171; positive cooperativity between PD81723 and NECA was reduced upon alanine substitution of a number of ECL2 residues, including $E170^{ECL2}$, and $K173^{ECL2}$, whereas mutation of $W146^{ECL2}$ and $W156^{ECL2}$ decreased VCP171 cooperativity with NECA. Molecular modeling localized a likely allosteric pocket for both modulators to an extracellular vestibule that overlaps with a region utilized by orthosteric ligands as they transit into the canonical A_1AR orthosteric site. MD simulations confirmed a key interaction between $E172^{ECL2}$ and both modulators. Bound PD81723 is flanked by another residue, $E170^{ECL2}$, which forms hydrogen bonds with adjacent $K168^{ECL2}$ and $K173^{ECL2}$. Collectively, our data suggest $E172^{ECL2}$ is a key allosteric ligand-binding determinant, whereas hydrogen-bonding networks within the extracellular vestibule may facilitate the transmission of cooperativity between orthosteric and allosteric sites.

Molecular Pharmacology Fast Forward. Published on September 28, 2016 as DOI: 10.1124/mol.116.105015
This article has not been copyedited and formatted. The final version may differ from this version.

Introduction

G protein-coupled receptors (GPCRs) account for approximately 30% of the targets of prescription medicines (Overington *et al.*, 2006). The majority of these medicines act at the endogenous agonist (orthosteric) site, however in many cases, orthosteric-based drug discovery remains suboptimal owing to lack of sufficient selectivity between related GPCR subtypes (May *et al.*, 2007b). One promising approach for achieving greater selectivity is to target topographically distinct allosteric sites on GPCRs (Christopoulos, 2002; May *et al.*, 2007b; Wootten *et al.*, 2013). Allosteric ligands have the potential to modulate the binding and/or signaling properties of an orthosteric ligand, and/or modulate GPCR activity even in the absence of orthosteric ligand (May and Christopoulos, 2003; Christopoulos, 2014). Allosteric regions typically display greater sequence divergence across the GPCR subtypes; enabling greater subtype selectivity when compared to the orthosteric domains. An additional advantage is that many allosteric modulators can selectively "tune" tissue responses either up or down when and where the endogenous agonist is present. This type of spatial and temporal specificity of action that can be achieved with allosteric modulators is unattainable with orthosteric ligands, which continuously stimulate or inhibit receptor function where and when they are present (Christopoulos and Kenakin, 2002; May *et al.*, 2007b).

The endogenous nucleoside, adenosine, acts via four adenosine GPCRs (ARs), the A_1AR, A_{2A}AR, A_{2B}AR, and A_3AR (Fredholm *et al.*, 2001). The highly subtype selective A_1AR allosteric ligand, PD81723 (2-amino-4,5-dimethyl-3-thienyl)-[3-(trifluoromethyl)phenyl]methanone), was the first synthetic positive allosteric modulator (PAM) of GPCR agonist function identified (Fig. 1) (Bruns and Fergus, 1990; Bruns *et al.*, 1990; May *et al.*, 2010; Hill *et al.*, 2014). The utility of A_1AR PAMs has been demonstrated in the kidney (Park *et al.*, 2012), heart (Bruns and Fergus, 1990; Valant *et al.*, 2010) and neurons (Pan *et al.*, 2001; Imlach *et al.*, 2015), suggesting that A_1AR PAMs provide a promising therapeutic avenue to treat renal and myocardial ischemia-reperfusion injury and chronic neuropathic pain. Given their therapeutic potential, numerous studies have investigated

Molecular Pharmacology Fast Forward. Published on September 28, 2016 as DOI: 10.1124/mol.116.105015
This article has not been copyedited and formatted. The final version may differ from this version.

the structure-activity relationships of A_1AR PAMs, predominantly exploring derivatives based on the 2-amino-3-benzoylthiophene scaffold (Romagnoli *et al.*, 2015). However, despite extensive derivation and interrogation of this core scaffold for over two decades, existing A_1ARs PAMs display largely low affinity, low cooperativity and generally poor solubility.

Alternative approaches, such as structure-based studies, are thus required to assist the design of more potent, selective and efficacious A_1AR modulators. The recent high-resolution A_{2A}AR crystal structures in both antagonist- and agonist-bound conformations have facilitated the generation of A_1AR homology models (Jaakola *et al.*, 2008; Xu *et al.*, 2011; Doré *et al.*, 2011; Lebon *et al.*, 2011). However, there remains a relative paucity of information regarding the location of the A_1AR allosteric site. This reflects key challenges associated with structure-function analyses of allostery, because the observed effect of any modulator in the presence of orthosteric ligand reflects a composite of at least three molecular properties: the *affinity* of the modulator for the unoccupied receptor, the *cooperativity* between the modulator and the orthosteric ligand when both are present, and the potential *intrinsic signaling efficacy* of each ligand; these properties can be governed by separate structure-activity and structure-function relationships (Christopoulos, 2014). Surprisingly, to date, only two structure-function studies have attempted to map the A_1AR allosteric site, both of which implicated the second extracellular loop (ECL2) of the A_1AR (specifically residues $W156^{ECL2}$, $E164^{ECL2}$, $S150^{ECL2}$ and $M162^{ECL2}$) in A_1AR PAM activity (Peeters *et al.*, 2012; Kennedy *et al.*, 2014). However, neither study explicitly addressed which residues governed modulator affinity relative to transmission of cooperativity or direct allosteric agonism. Nonetheless, this work clearly highlighted ECL2 as important in the actions of the subtype selective 2-amino-3-benzoylthiophene A_1AR allosteric modulators, as this region is the least conserved in both sequence and length across the AR subtypes.

In our accompanying article (Nguyen *et al.*, 2016), we demonstrated that ECL2 can significantly

Molecular Pharmacology Fast Forward. Published on September 28, 2016 as DOI: 10.1124/mol.116.105015
This article has not been copyedited and formatted. The final version may differ from this version.

influence orthosteric agonist and antagonist pharmacology. Furthermore, ECL2 is involved in the "transit" of agonists into the orthosteric site within the transmembrane (TM) domains. Herein we assessed the influence of select A_1AR-ECL2 alanine mutations on the affinity, cooperativity and efficacy of the well-characterized allosteric enhancer, PD81723, and a more recent derivative, VCP171 ((2-amino-4-(3-(trifluoromethyl)phenyl)thiophen-3-yl)(phenyl)methanone) (Fig. 1) (Aurelio *et al.*, 2009b). We find that ECL2 contributes to a common allosteric pocket in the extracellular vestibule that overlaps with the transit pocket utilized by orthosteric ligands, identify $E172^{ECL2}$ as a vital residue for modulator affinity, and highlight how different residues can mediate cooperativity and direct agonism in a manner that can vary with the nature of the allosteric or orthosteric ligand under investigation.

Molecular Pharmacology Fast Forward. Published on September 28, 2016 as DOI: 10.1124/mol.116.105015
This article has not been copyedited and formatted. The final version may differ from this version.

Materials and Methods

Materials

VCP171 was synthesized as described previously (Aurelio *et al.*, 2009b; Valant *et al.*, 2014). PD81723 was synthesized as described previously (Aurelio *et al.*, 2009a). All other reagents were obtained from suppliers described in the accompanying article (Nguyen *et al.*, 2016).

Receptor Mutagenesis, Transfection, Cell Culture and Receptor Expression

Receptor mutagenesis, transfection, cell culture and measurement of cell surface expression of wild-type (WT) and mutant human A_1ARs containing a triple human influenza hemagglutinin (HA) N-terminal tag (3xHA-A_1ARs) was performed as described in our accompanying article (Nguyen *et al.*, 2016).

Whole cell radioligand binding

[^{3}H]DPCPX (8-cyclopentyl-1,3-dipropylxanthine, [dipropyl-2,3-^{3}H(N)]) whole cell interaction binding assays on Chinese hamster ovary (CHO) Flp-In™ cells stably expressing the WT or mutant 3xHA-A_1AR were performed at 4^{o}C for 3 h in a final volume of 100 μL HEPES buffer (145 mM NaCl, 10 mM D-Glucose, 5 mM KCl, 1 mM $MgSO_4$, 10 mM HEPES, 1.3 mM $CaCl_2$, 15 mM $NaHCO_3$, pH 7.45) in the presence of 1 nM [^{3}H]DPCPX, increasing concentrations of the orthosteric agonist 5'-*N*-ethylcarboxamidoadenosine (NECA) and/or allosteric ligand (PD81723 or VCP171). Nonspecific binding was defined with 1 μM of selective A_1AR antagonist *trans*-4-[(2-phenyl-7*H*-pyrrolo[2,3-*d*]pyrimidin-4-yl)amino]cyclohexanol. Assays were then terminated by washing twice with 100 μL cold phosphate buffered saline (PBS)/well, followed by the addition of 100 μL OptiPhase Supermix™ scintillation cocktail and bound radioactivity was measured using a MicroBeta^2 ™ plate counter (PerkinElmer).

Inhibition of cAMP accumulation

Molecular Pharmacology Fast Forward. Published on September 28, 2016 as DOI: 10.1124/mol.116.105015
This article has not been copyedited and formatted. The final version may differ from this version.

Inhibition of cAMP accumulation was assessed as described previously (Baltos *et al.*, 2016). Briefly, Flp-In™-CHO cells stably expressing the WT or mutant 3xHA-A_1AR were seeded at 20,000 cells/well in a 96-well plate and incubated at 37°C overnight. Interaction assays were performed at 37°C in stimulation buffer (140 mM NaCl, 5.4 mM KCl, 0.8 μM $MgSO_4$, 0.2 mM Na_2HPO_4, 0.44 mM KH_2PO_4, 1.3 mM $CaCl_2$, 5.6 mM D-glucose, 5 mM HEPES, 0.1% bovine serum albumin, and 10 μM rolipram, pH 7.45). Cells were washed and incubated in stimulation buffer for 30 min, followed by a 10 min exposure to allosteric modulator alone and then the addition of 3 μM forskolin in the absence and presence of increasing concentrations of NECA. Following a 30 min incubation at 37°C, the reaction was terminated by rapid removal of buffer and the addition of 50 μL of ice-cold ethanol. Following ethanol evaporation, detection was performed as outlined previously (Baltos *et al.*, 2016; Vecchio *et al.*, 2016).

Data Analysis

Data were analyzed using nonlinear regression analysis software (GraphPad Prism 6.0). Equilibrium binding interaction experiments were fitted to the following allosteric ternary complex model (Leach *et al.*, 2010):

$$Y = \frac{B_{max}[A]}{[A] + \left(\frac{K_A K_B}{\alpha_A [B] + K_B}\right)\left(1 + \frac{[I]}{K_I} + \frac{[B]}{K_B} + \frac{\alpha_I [I][B]}{K_I K_B}\right)} \qquad \text{(Equation 1)}$$

where Y is specific binding, B_{max} is the relative receptor expression, K_A , K_B , and K_I represent the equilibrium dissociation constants of [^{3}H]DPCPX (A), the allosteric ligand (B) and NECA (I), respectively. The binding cooperativity between the allosteric ligand and [^{3}H]DPCPX or NECA are denoted by α_A or α_I, respectively. A cooperativity factor $\alpha > 1$ describes positive cooperativity; a value $0 < \alpha < 1$ describes negative cooperativity, and a value of $\alpha = 1$ describes neutral cooperativity.

Molecular Pharmacology Fast Forward. Published on September 28, 2016 as DOI: 10.1124/mol.116.105015
This article has not been copyedited and formatted. The final version may differ from this version.

Concentration-response curves for the interaction between NECA and allosteric ligands, PD81723 and VCP171, in a cAMP accumulation assay were globally fitted to the following operational model of allosterism (Leach *et al.*, 2007):

$$E = \frac{E_m\left(\tau_A[A]\left(K_B + \alpha\beta[B]\right) + \tau_B[B]K_A\right)^n}{\left([A]K_B + K_AK_B + [B]K_A + \alpha[A][B]\right)^n + \left(\tau_A[A]\left(K_B + \alpha\beta[B]\right) + \tau_B[B]K_A\right)^n} \quad \text{(Equation 2)}$$

where E_m is the maximal cellular response, K_A and K_B are the equilibrium dissociation constants of NECA (A) and the allosteric ligand (B), respectively, τ_A and τ_B are operational measures of NECA and allosteric ligand efficacy, respectively, α is the binding cooperativity factor and β denotes the magnitude of the allosteric effect on orthosteric agonist efficacy, and n is the slope of the transducer function that links occupancy to response. Orthosteric agonist and allosteric ligand affinity were constrained to values determined from radioligand binding (Table 1 and accompanying article). Efficacy parameters (τ_A and τ_B) were corrected for differences in receptor expression between mutants by using the B_{max} values determined from saturation binding assays to scale the efficacy (τ) parameters to that of the wild type receptor (Gregory *et al.*, 2010). All data preferentially fitted to a transducer slope (n) equal to 1, as determined by an extra-sum-of-squares (F test).

All values of potency, affinity, efficacy and cooperativity were estimated as logarithms (Christopoulos, 1998). Statistical analysis was performed using a one-way analysis of variance with a Dunnet's post-hoc test to determine differences between the WT and mutant 3xHA-A_1AR mutants. Statistical significance was defined as $P < 0.05$.

Homology Modeling, Docking and Molecular Dynamics Simulations

The generation of the active-like homology model of the A_1AR based on the agonist-bound human

Molecular Pharmacology Fast Forward. Published on September 28, 2016 as DOI: 10.1124/mol.116.105015
This article has not been copyedited and formatted. The final version may differ from this version.

A_{2A}AR (PDB ID 3QAK) was described in our accompanying article (Nguyen *et al.,* 2016). The ICM Pocket Finder algorithm was used to predict potential ligand binding sites, and NECA, PD81723 and VCP171 were docked using ICM version 3.8.0 (with default parameters) (An *et al.*, 2005; Abagyan and Kufareva, 2009). The top scoring docking conformation for each ligand was selected and prepared for MD simulations. MD simulations of the final complex were carried out with the NAMD 2.10 (Phillips *et al.*, 2005) package using the 3-site rigid water TIP3P model, CHARMM27 (MacKerell *et al.*, 1998; Mackerell *et al.*, 2004), and CGenFF (Vanommeslaeghe *et al.*, 2010; Yu *et al.*, 2012) v.3.0.1 force fields as described previously (Aksimentiev *et al.*, 2012; Shonberg *et al.*, 2013). The particle mesh Ewald (PME) (Essmann *et al.*, 1995) method was used to evaluate electrostatic interactions. Each system contained an A_1AR, NECA and either PD81723 or VCP171, in the presence of a lipid bilayer composed of ~220 1-palmitoyl-2-oleoyl-sn-glycero-3-phosphocholine (POPC) molecules generated using the membrane plugin of the VMD software (v1.9.2) (Humphrey *et al.*, 1996), and ~15800 water molecules. Sodium and chloride ions were added to neutralize the system, with extra NaCl added to reach a final concentration of 150 mM (~35 sodium ions, ~48 chloride ions). MD energy minimization, equilibration and the production run were performed as described within the accompanying manuscript. VMD v1.9.2 was used for the visualization and analysis of the residue-ligand contacts through the course of each simulation using in-house scripts.

Molecular Pharmacology Fast Forward. Published on September 28, 2016 as DOI: 10.1124/mol.116.105015
This article has not been copyedited and formatted. The final version may differ from this version.

Results

Expression of human A_1AR ECL2 alanine mutants

As reported in our accompanying article that investigated the role of ECL2 on orthosteric ligand pharmacology (Nguyen *et al.,* 2016), each residue within ECL2 was substituted for alanine, with the exception of $C169^{ECL2}$, which is known to form an important disulfide bond with $C80^{3.35}$ in TM3. Superscripts refer to Ballesteros-Weinstein residue numbering (Ballesteros and Weinstein, 1995). Alanine substitutions were made in the 3xHA-A_1AR, that is a human A_1AR containing a triple HA N-terminal tag. The pharmacology of the allosteric ligands, PD81723 and VCP171, was equivalent at the 3xHA-A_1AR and untagged human A_1AR (data not shown). In all cases, single alanine mutations were introduced, with the exception of $S150^{ECL2}$A + $V151^{ECL2}$A ($SV150^{ECL2}$AA) and $M162^{ECL2}$A + $G163^{ECL2}$A + $E163^{ECL2}$A ($MGE162^{ECL2}$AAA), for which double and triple mutations were substituted and well expressed. Furthermore as outlined within our accompanying article (Nguyen *et al.,* 2016), although the 3xHA-A_1AR containing the alanine substitution of $F171^{ECL2}$ was expressed to similar levels as the WT (Supplemental Fig.1 of accompanying manuscript), orthosteric ligand binding and function could not be detected and therefore this mutation was not investigated in the current study.

The influence of A_1AR-ECL2 alanine substitutions on allosteric ligand affinity and cooperativity

Whole cell [^{3}H]DPCPX interaction binding assays in the absence and presence of increasing concentrations of the orthosteric agonist, NECA, and allosteric ligands were performed at WT and mutant 3xHA-A_1AR (Fig. 2A & B). Fitting of these data to an allosteric ternary complex model allowed estimation of allosteric ligand affinity (pK_B) and binding cooperativity ($log\alpha_I$) between the allosteric ligand and orthosteric agonist (Table 1); in most cases, the cooperativity between the modulators and [^{3}H]DPCPX was highly negative and thus the value of $log\alpha_A$ was constrained to a very low value of -3 (i.e., $\alpha_A = 0.001$, making it indistinguishable from competitive inhibition). At the WT 3xHA-A_1AR, PD81723 and VCP171 had micromolar affinity for the allosteric site on the

Molecular Pharmacology Fast Forward. Published on September 28, 2016 as DOI: 10.1124/mol.116.105015
This article has not been copyedited and formatted. The final version may differ from this version.

unoccupied receptor, and enhanced the affinity of NECA approximately 4-8 fold, depending on the PAM. The only mutation that resulted in a significant decrease in the affinity of PD81723 and VCP171 for the free (unoccupied) receptor was E172^{ECL2}A (Fig. 3). Indeed, E172^{ECL2}A was the only ECL2 mutation to significantly influence VCP171 affinity, albeit to a lesser extent than PD81723 (Fig. 3B). In contrast, an increase in the affinity of PD81723 was observed upon alanine substitution of nine residues, N147^{ECL2}, N148^{ECL2}, S161^{ECL2}, V166^{ECL2}, I167^{ECL2}, K168^{ECL2}, E170^{ECL2}, K173^{ECL2} and I175^{ECL2} (Fig. 3A).

The ECL2 mutations that significantly influenced allosteric binding cooperativity with the orthosteric agonist NECA were probe-dependent, that is, not conserved between PD81723 and VCP171. With respect to PD81723, three pairs of mutations significantly decreased PD81723 binding cooperativity with the agonist, namely, N147^{ECL2}A and N148^{ECL2}A; G160^{ECL2}A and S161^{ECL2}A; E170^{ECL2}A and K173^{ECL2}A (Fig. 3A). With the exception of G160^{ECL2}, each of these mutations was also associated with a concurrent increase in PD81723 affinity. With respect to VCP171, alanine substitution of two tryptophan residues, W146^{ECL2} and W156^{ECL2}, caused a significant decrease in the binding cooperativity between VCP171 and NECA, with no significant effect on VCP171 affinity (Fig. 3B). For comparison, the composite parameter, $\log\alpha_I+pK_B$, which reflects the affinity of each modulator on the NECA-occupied receptor, is also shown in Table 1, where it can be seen that far more subtle effects of each mutation would be concluded if the individual contributions of amino acids to the affinity for the unoccupied receptor relative to cooperativity were not evaluated.

The influence of ECL2 alanine substitutions on allosteric ligand efficacy and functional cooperativity with NECA

Functional interaction assays in the absence and presence of increasing concentrations of orthosteric agonist and/or allosteric ligands were performed at WT and mutant 3xHA-A_1AR (Fig. 2C & D).

Molecular Pharmacology Fast Forward. Published on September 28, 2016 as DOI: 10.1124/mol.116.105015
This article has not been copyedited and formatted. The final version may differ from this version.

Data were fitted to an operational model of allosterism to estimate allosteric ligand efficacy corrected for changes in receptor expression ($\log\tau_{B(C)}$) and functional cooperativity ($\log\alpha\beta$) between the allosteric ligand and the orthosteric agonist, NECA (Table 2). Functional interaction assays performed in the absence and presence of adenosine deaminase were comparable, suggesting minimal influence of endogenous adenosine (unpublished results). Similar to previous findings for Flp-In™-CHO cells stably expressing the wild-type A_1AR (Vecchio *et al.*, 2016), no evidence for constitutive activity was apparent for wild-type or mutant A_1ARs (unpublished results).

In the absence of orthosteric agonist, both PD81723 and VCP171 behaved as allosteric partial agonists at the WT 3xHA-A_1AR, mediating an increase in the inhibition of forskolin-stimulated cAMP accumulation (Fig. 2C, D). Analysis of interaction experiments between increasing concentrations of each modulator and NECA found that residues involved in the transmission of direct allosteric ligand efficacy ($\tau_{B(C)}$) were relatively conserved between PD81723 and VCP171. A significant decrease in the efficacy of PD81723 and VCP171 was observed at N148^{ECL2}A, E153^{ECL2}A, S161^{ECL2}A and I167^{ECL2}A (Fig. 3). A five- to ten-fold decrease in efficacy of PD81723 and VCP171 was also observed at R154^{ECL2}A and I175^{ECL2}A, however this only reached significance for VCP171 (Fig. 3). Both PAMs enhanced NECA potency at the WT 3xHA-A_1AR approximately 4-fold. Interestingly, while E172^{ECL2}A caused a small increase in the functional cooperativity ($\log\alpha\beta$) between PD81723 and the agonist (Fig. 3A), the remaining mutations had no significant effect. For VCP171, two clusters of ECL2 mutations caused a small but significant decrease in VCP171 functional cooperativity. The first cluster involved R154^{ECL2}A, W156^{ECL2}A and N159^{ECL2}A, and the second involved V174^{ECL2}A and I175^{ECL2}A (Fig. 3B). These results may suggest a divergence in the influence of the mutations on cooperativity with NECA at the level of binding affinity (α) versus efficacy (β). However, evaluation of $\log(\beta)$ values found no significant difference from the WT, with the exception of the influence of S161^{ECL2}A on PD81723, suggesting

Molecular Pharmacology Fast Forward. Published on September 28, 2016 as DOI: 10.1124/mol.116.105015
This article has not been copyedited and formatted. The final version may differ from this version.

that the observed cooperativity between NECA and the modulators is largely driven by changes in binding cooperativity (α) (Supplemental Fig. 1A).

Molecular modeling of the A_1AR allosteric site

As described in the accompanying manuscript (Nguyen *et al.,* 2016), an "active-like" homology model of the human A_1AR was generated based on the agonist (UK432097)-bound human A_{2A}AR crystal structure. The ICM PocketFinder software identified three potential binding pockets within this model. One pocket was located within the TM bundle and corresponded to the well-characterized deep orthosteric site, whereas the other two pockets were located within different regions of the extracellular vestibule. NECA was docked into the deep orthosteric pocket in the TM region and the allosteric modulators were docked into the putative allosteric sites within the extracellular vestibule. MD simulations were performed for each A_1AR homology model co-bound with the NECA and either PAM. When PD81723 or VCP171 were docked into the pocket located exclusively within ECL2, both PAMs dissociated from the binding site in four of the five 10 ns MD simulations. Furthermore, this binding pocket does not involve $E172^{ECL2}$, the only ECL2 residue that significantly decreased A_1AR allosteric ligand affinity when mutated to alanine. Collectively, these results suggest this pocket is unlikely to represent the A_1AR allosteric binding site.

The second putative allosteric pocket was located within the extracellular vestibule bordered by TM2, ECL2, TM6, ECL3 and TM7 (colored red in Fig. 4). PD81723 and VCP171 were more stable in this pocket, remaining bound during the entire 40 ns MD simulation in all but one of the 7 MD simulations (Fig. 5). Residues located within 3.5 Å of PD81723 for an average 60-70% of the 40 ns run-time for each of the six MD simulations were $F171^{ECL2}$, $E172^{ECL2}$ and $N254^{6.55}$ (Fig. 6A). Within the extracellular vestibule, PD81723 was predicted to form hydrogen bonds with $E172^{ECL2}$ with the highest frequency compared to the other residues (Fig. 7; Data Supplement 1), which correlates well with the significant reduction in PD81723 affinity observed for the $E172^{ECL2}$A

Molecular Pharmacology Fast Forward. Published on September 28, 2016 as DOI: 10.1124/mol.116.105015
This article has not been copyedited and formatted. The final version may differ from this version.

mutation (Fig. 7C). PD81723 was also flanked by a hydrogen bond with the side chain of another glutamic acid residue, $E170^{ECL2}$ (Fig. 7B). This residue was found to reside within 3.5 Å of PD81723 for greater than 20% of total MD time in two of the six simulations (Fig. 6A). Our molecular modeling predicted a network of hydrogen bond interactions between residues within the extracellular vestibule surrounding the allosteric binding pocket (Fig. 7B). These include a hydrogen bond between $E172^{ECL2}$ and $K265^{ECL3}$ as well as a hydrogen bond between the side chain of $E170^{ECL2}$ and two lysine residues $K168^{ECL2}$ and $K173^{ECL2}$ (Fig. 7B). Our mutagenesis results suggest that both $E170^{ECL2}$ and $K173^{ECL2}$ are involved in the transmission of PD81723 binding cooperativity (Fig. 7D). As such, in addition to stabilizing the A_1AR extracellular structure, the putative network of hydrogen bond interactions within the extracellular vestibule may have a role in the transmission of cooperativity between the extracellular and orthosteric binding sites. ECL2 residues located within 3.5 Å of VCP171 during the 40 ns MD simulations include $F171^{ECL2}$ and $E172^{ECL2}$ (Fig. 6B). Similar to PD81723, VCP171 was stabilized in the allosteric pocket via a hydrogen bond with $E172^{ECL2}$, the only residue for which a significant reduction in VCP171 affinity was observed upon mutation to alanine (Fig. 8; Data Supplement 2). Collectively, these MD simulations support our experimental finding that $E172^{ECL2}$ is a critical determinant for allosteric ligand binding.

Molecular Pharmacology Fast Forward. Published on September 28, 2016 as DOI: 10.1124/mol.116.105015
This article has not been copyedited and formatted. The final version may differ from this version.

Discussion

The A_1AR is a potential therapeutic target for a number of conditions. A_1AR allosteric modulators offer considerable advantages over their orthosteric counterparts, however, discovery efforts have yet to yield A_1AR-selective allosteric modulators with high affinity and/or substantially diverse chemotypes. Medicinal chemistry efforts can be enriched by efforts that allow localization of the A_1AR allosteric site coupled with delineation of structural determinants that govern affinity, cooperativity and efficacy of allosteric ligands. Numerous class A GPCR allosteric sites recognized by exogenous ligands are thought to reside within the extracellular vestibule (Voigtlander *et al.*, 2003; Avlani *et al.*, 2007; Jäger *et al.*, 2007; Narlawar *et al.*, 2010; Nawaratne *et al.*, 2010; Peeters *et al.*, 2012; Abdul-Ridha *et al.*, 2014). As such, the aim of the current study was to delineate the role of ECL2 in A_1AR allosteric ligand pharmacology. We performed an alanine scan of ECL2 and quantified the effect of mutations on allosteric ligand affinity, efficacy and cooperativity. Ligand docking and MD simulations were subsequently performed to assist with the interpretation of our findings. A negatively charged amino acid, $E172^{ECL2}$ was identified as a key ECL2 residue involved in the binding of two allosteric ligands, PD81723 and VCP171 to the unoccupied receptor. ECL2 was also found to be essential for the transmission of cooperativity and for direct allosteric ligand intrinsic efficacy.

To date, only a few studies have attempted to map the A_1AR allosteric site. Two recent structure-function studies implicated ECL2 (Peeters *et al.*, 2012; Kennedy *et al.*, 2014), however neither study differentiated residues involved in allosteric binding affinity versus cooperativity or efficacy. Peeters *et al.* (2012) suggested alanine substitution of $W156^{ECL2}$ decreased PD81723 allosteric activity. Our results suggest that the mechanism behind this effect is because $W156^{ECL2}$ is one of two tryptophan residues involved in mediating binding cooperativity between A_1AR PAMs and orthosteric agonists, in our case specifically between VCP171 and NECA (Fig. 8D, Fig. 8F). The recent high-resolution crystal structure of an active human M_2 muscarinic acetylcholine receptor

Molecular Pharmacology Fast Forward. Published on September 28, 2016 as DOI: 10.1124/mol.116.105015
This article has not been copyedited and formatted. The final version may differ from this version.

bound to both an orthosteric agonist and PAM identified extensive π-π stacking interactions between the aromatic ring of the PAM and aromatic residues in ECL2 and the top of TM7 (Kruse *et al*., 2013). Similar π-π stacking interactions may occur between the aromatic rings of VCP171 and the tryptophan residues $W156^{ECL2}$ and $W146^{ECL2}$ in the A_1AR-ECL2, however long time-scale MD simulations may be required to observe such interactions. A second study by Kennedy *et al.* (2014) combined alanine scanning and radioligand dissociation kinetic assays with molecular modeling and observed a significant decrease in A_1AR PAM, ATL525 (2-amino-4,5,6,7-tetrahydro-benzo[b]thiophen-3-yl) biphenyl-4-yl-methanone), activity at two constructs containing alanine mutations within ECL2: N147+N148+L149+S150 and N159+G160+S161+M162. In agreement with these results, we observed a significant decrease in the binding cooperativity between PD81723 and NECA upon single alanine substitution of $N147^{ECL2}$, $N148^{ECL2}$, $G160^{ECL2}$ or $S161^{ECL2}$. In contrast with our results, Kennedy *et al* (2014) identified $S150^{ECL2}$ and $M162^{ECL2}$ as key residues involved in conferring allosteric activity of ATL525. However, we have shown that the residues involved in the transmission of allosteric cooperativity appear to be probe-dependent. This probe dependence may be due to actual differences in binding modes/poses or, as suggested by our current work, due to differences in the transmission of cooperativity from a "common" allosteric binding domain.

The combination of our mutational and computational data suggests that $E172^{ECL2}$ is a key residue involved in binding of both PD81723 and VCP171 to the non-agonist-occupied A_1AR. The putative allosteric site was bordered by $E172^{ECL2}$. The 2-amino and 3-keto group of PD81723 and VCP171 were predicted to form hydrogen bond interactions with $E172^{ECL2}$ during MD simulations of co-bound orthosteric and allosteric ligands; both the 2-amino and 3-keto groups are known to be required for A_1AR allosteric ligand activity (Bruns *et al.*, 1990; Kennedy *et al*., 2014). Of particular note, this proposed allosteric binding pocket, supported by our experimental findings and MD, overlaps with the "transition site" within the extracellular vestibule proposed for the orthosteric

Molecular Pharmacology Fast Forward. Published on September 28, 2016 as DOI: 10.1124/mol.116.105015
This article has not been copyedited and formatted. The final version may differ from this version.

agonist, NECA, and partially overlaps with the binding site of the orthosteric antagonist, DPCPX, in our accompanying manuscript (Nguyen *et al.*, 2016). This finding may explain prior studies where relatively subtle structural changes in A_1AR molecules can convert allosteric modulators into compounds with apparently orthosteric pharmacology, i.e., these changes can alter the thermodynamic properties that favor recognition of one pocket over the other (Aurelio *et al.*, 2010; 2011; Valant *et al.*, 2012). Furthermore, the predicted partial overlap between the putative allosteric pocket and DPCPX provides a potential mechanism to explain the previously proposed competitive interaction between A_1AR allosteric modulators and orthosteric antagonists (Bruns *et al.*, 1990), as well as our findings of an inhibitory interaction between either PD81723 or VCP171 with [^{3}H]DPCPX.

Prior studies of the M_2 muscarinic acetylcholine receptor also identified a role for charged residues within ECL2 in the affinity and/or cooperativity of allosteric ligands (Gnagey *et al.*, 1999; May *et al.*, 2007a). In our study, alanine substitution of the charged A_1AR ECL2 residues, E170^{ECL2} and K173^{ECL2}, significantly decreased the positive cooperativity between the NECA and PD81723. Furthermore, alanine substitution of E172^{ECL2} significantly decreased allosteric ligand affinity. Interestingly, at both the A_1AR and M_2 receptor, the cluster of charged residues implicated in allosteric ligand binding and/or the transmission of cooperativity is proximal to the conserved cysteine residue within ECL2 that forms a disulfide bond with TM3. Furthermore, our molecular modeling suggests multiple negatively charged glutamic acid and positively charged lysine residues located within the extracellular vestibule are involved in a network of hydrogen bonds. During MD simulations, the side chain of E170^{ECL2} forms a hydrogen bond with PD81723 and the side chain of two adjacent lysine residues, K168^{ECL2} and K173^{ECL2}. Further, E172^{ECL2} also makes a hydrogen bond with K265^{ECL3}, shaping the extracellular region of the A_1AR. These findings further highlight the potential role of charged residues within the extracellular vestibule in allosteric ligand actions at the A_1AR. .

Molecular Pharmacology Fast Forward. Published on September 28, 2016 as DOI: 10.1124/mol.116.105015
This article has not been copyedited and formatted. The final version may differ from this version.

The positive binding cooperativity for PD81723 was substantially reduced upon alanine substitution of $N147^{ECL2}$, $N148^{ECL2}$, $G160^{ECL2}$ and $S161^{ECL2}$. Glycine is the smallest amino acid due to the lack of a side chain. Consequently, this amino acid has the greatest conformational flexibility, a mobility that may be required for the transmission of cooperativity. The polar asparagine and serine residues implicated in the transmission of cooperativity are located relatively far from the predicted allosteric site, and therefore likely have indirect effects. Alternatively, the middle section of ECL2 may form a lid over the allosteric binding site and stabilize the conformation of the allosteric pocket. However, such large-scale movements are unlikely to be observed during the 40 ns MD simulations.

Nonetheless, the use of analytical approaches that differentiate mutational effects on modulator affinity from those that govern allosteric efficacy or that mediate the transmission of cooperativity with orthosteric ligands raises at least two key issues for future consideration, both related to the role of the transition of the unliganded receptor to a bound active state. The first issue is exemplified by the decrease in signaling efficacy of both PD81723 and VCP171 upon alanine substitution of $N148^{ECL2}$, $E153^{ECL2}$, $R154^{ECL2}$, $S161^{ECL2}$, $I167^{ECL2}$ or $I175^{ECL2}$. In our accompanying article (Nguyen *et al.*, 2016), a significant decrease in the efficacy of the orthosteric agonist, NECA, was also observed at the $N148^{ECL2}$A, $E153^{ECL2}$A and $R154^{ECL2}$ mutations, suggesting that these residues are part of a "global" activation mechanism irrespective of the "trigger" (i.e., allosteric or orthosteric). In contrast, $S161^{ECL2}$, $I167^{ECL2}$ and $I175^{ECL2}$ appear to be exclusively involved in the transmission of allosteric but not orthosteric ligand efficacy. The paradigm of global versus allosteric modulator-specific activation mechanisms has been reported for other receptors (e.g., Nawaratne *et al.*, 2010). The second key issue relates to mechanisms underlying the transmission of cooperativity. Although our mutational analysis of modulator affinity was determined explicitly within the context of the free receptor, changes in cooperativity reflect effects on the ternary

Molecular Pharmacology Fast Forward. Published on September 28, 2016 as DOI: 10.1124/mol.116.105015
This article has not been copyedited and formatted. The final version may differ from this version.

complex of agonist-receptor-modulator. It is likely that the nature of the allosteric pocket changes dramatically between the two states; this would not be captured by the ground state K_B value, but would be subsumed in the cooperativity values. Thus, the hydrogen bond networks implicated as playing a role in the transmission of allostery may be part of a larger, more dynamic, network that reflects receptor transition between states, and to which ECL2 contributes an important role. This can also explain why some of the residues that have a significant effect on ligand pharmacology, particularly signaling efficacy or cooperativity, need not be in the immediate vicinity of any predicted binding pocket.

In conclusion, the current study has provided new insights into the location of the A_1AR allosteric site, as well as residues involved in the transmission of allosteric cooperativity and efficacy. Residues involved in allosteric ligand binding and efficacy were conserved between the two allosteric ligands assessed, whereas residues involved in the transmission of allosteric cooperativity were distinct. The delineation of ECL2 residues involved in allosteric ligand affinity, cooperativity and efficacy provided within this study may facilitate future structure-function studies of the A_1AR allosteric site and assist structure-based design of novel A_1AR allosteric ligands.

Molecular Pharmacology Fast Forward. Published on September 28, 2016 as DOI: 10.1124/mol.116.105015
This article has not been copyedited and formatted. The final version may differ from this version.

Acknowledgements

The authors thank Mr Thomas Coudrat for assistance with molecular modeling.

Molecular Pharmacology Fast Forward. Published on September 28, 2016 as DOI: 10.1124/mol.116.105015
This article has not been copyedited and formatted. The final version may differ from this version.

Authorship contributions

Participated in research design: ATNN, PMS, LTM, AC

Conducted experiments: ATNN, EAV, LA

Performed data analysis: ATNN, TDN, TT

Wrote or contributed to the writing of the manuscript: ATNN, KJG, PJW, PJS, PMS, LTM, AC

Molecular Pharmacology Fast Forward. Published on September 28, 2016 as DOI: 10.1124/mol.116.105015
This article has not been copyedited and formatted. The final version may differ from this version.

References

Abagyan R, and Kufareva I (2009) The flexible pocketome engine for structural chemogenomics. *Methods Mol Biol* **575**:249–279.

Abdul-Ridha A, López L, Keov P, Thal DM, Mistry SN, Sexton PM, Lane JR, Canals M, and Christopoulos A (2014) Molecular Determinants of Allosteric Modulation at the M_1 Muscarinic Acetylcholine Receptor. *J Biol Chem* **289**:6067–6079.

Aksimentiev A, Sotomayor M, and Wells D (2012) Membrane proteins tutorial. http://www.ks.uiuc.edu/Training/Tutorials/science/membrane/mem-tutorial.pdf

An J, Totrov M, and Abagyan R (2005) Pocketome via comprehensive identification and classification of ligand binding envelopes. *Mol Cell Proteomics* **4**:752–761.

Aurelio L, Christopoulos A, Flynn BL, Scammells PJ, Sexton PM, and Valant C (2011) The synthesis and biological evaluation of 2-amino-4,5,6,7,8,9-hexahydrocycloocta[b]thiophenes as allosteric modulators of the A_1 adenosine receptor. *Bioorg Med Chem Lett* **21**:3704–3707.

Aurelio L, Flynn BL, and Scammells PJ (2009a) Reaction Pathways to 2-Aminothiophenes and Thiophene-3-carbonitriles. *Aust J Chem* **62**:402–406.

Aurelio L, Valant C, Flynn BL, Sexton PM, Christopoulos A, and Scammells PJ (2009b) Allosteric Modulators of the Adenosine A_1 Receptor: Synthesis and Pharmacological Evaluation of 4-Substituted 2-Amino-3-benzoylthiophenes. *J Med Chem* **52**:4543–4547.

Aurelio L, Valant C, Flynn BL, Sexton PM, White JM, Christopoulos A, and Scammells PJ (2010) Effects of conformational restriction of 2-amino-3-benzoylthiophenes on A(1) adenosine receptor modulation. *J Med Chem* **53**:6550–6559.

Avlani VA, Gregory KJ, Morton CJ, Parker MW, Sexton PM, and Christopoulos A (2007) Critical role for the second extracellular loop in the binding of both orthosteric and allosteric G protein-coupled receptor ligands. *J Biol Chem* **282**:25677–25686.

Ballesteros J, and Weinstein H (1995) Integrated methods for the construction of three dimensional models and computational probing of structure function relations in G protein-coupled

receptors. *Methods Neurosci* **25**:366–428.

Baltos J-A, Gregory KJ, White PJ, Sexton PM, Christopoulos A, and May LT (2016) Quantification of adenosine A_1 receptor biased agonism: Implications for drug discovery. *Biochem Pharmacol* **99**:101–112.

Bruns RF, and Fergus JH (1990) Allosteric enhancement of adenosine A_1 receptor binding and function by 2-amino-3-benzoylthiophenes. *Mol Pharmacol* **38**:939–949.

Bruns RF, Fergus JH, Coughenour LL, Courtland GG, Pugsley TA, Dodd JH, and Tinney FJ (1990) Structure-activity relationships for enhancement of adenosine A_1 receptor binding by 2-amino-3-benzoylthiophenes. *Mol Pharmacol* **38**:950–958.

Christopoulos A (2014) Advances in G protein-coupled receptor allostery: from function to structure. *Mol Pharmacol* **86**:463–478.

Christopoulos A (2002) Allosteric binding sites on cell-surface receptors: novel targets for drug discovery. *Nat Rev Drug Discov* **1**:198–210.

Christopoulos A (1998) Assessing the distribution of parameters in models of ligand–receptor interaction: to log or not to log. *Trends Pharmacol Sci* **19**:351–357.

Christopoulos A, and Kenakin T (2002) G protein-coupled receptor allosterism and complexing. *Pharmacol Rev* **54**:323–374.

Doré AS, Robertson N, Errey JC, Ng I, Hollenstein K, Tehan B, Hurrell E, Bennett K, Congreve M, Magnani F, Tate CG, Weir M, and Marshall FH (2011) Structure of the Adenosine A_{2A} Receptor in Complex with ZM241385 and the Xanthines XAC and Caffeine. *Structure* **19**:1283–1293.

Essmann U, Perera L, Berkowitz ML, Darden T, Lee H, and Pedersen LG (1995) A smooth particle mesh Ewald method. *J Chem Phys* **103**:8577–8593.

Fredholm BB, IJzerman AP, Jacobson KA, Klotz K-N, and Linden J (2001) International Union of Pharmacology. XXV. Nomenclature and Classification of Adenosine Receptors. *Pharmacol Rev* **53**:527–552.

Gnagey AL, Seidenberg M, and Ellis J (1999) Site-directed mutagenesis reveals two epitopes involved in the subtype selectivity of the allosteric interactions of gallamine at muscarinic acetylcholine receptors. *Mol Pharmacol* **56**:1245–1253.

Gregory KJ, Hall NE, Tobin AB, Sexton PM, and Christopoulos A (2010) Identification of orthosteric and allosteric site mutations in M_2 muscarinic acetylcholine receptors that contribute to ligand-selective signaling bias. *J Biol Chem* **285**:7459–7474.

Hill SJ, May LT, Kellam B, and Woolard J (2014) Allosteric interactions at adenosine A_1 and A_3 receptors: new insights into the role of small molecules and receptor dimerization. *Br J Pharmacol* **171**:1102–1113.

Humphrey W, Dalke A, and Schulten K (1996) VMD: visual molecular dynamics. *J Mol Graph* **14**:33–38.

Imlach WL, Bhola RF, May LT, Christopoulos A, and Christie MJ (2015) A Positive Allosteric Modulator of the Adenosine A_1 Receptor Selectively Inhibits Primary Afferent Synaptic Transmission in a Neuropathic Pain Model. *Mol Pharmacol* **88**:460–468.

Jaakola V-P, Griffith MT, Hanson MA, Cherezov V, Chien EYT, Lane JR, IJzerman AP, and Stevens RC (2008) The 2.6 Angstrom Crystal Structure of a Human A_{2A} Adenosine Receptor Bound to an Antagonist. *Science* **322**:1211–1217.

Jäger D, Schmalenbach C, Prilla S, Schrobang J, Kebig A, Sennwitz M, Heller E, Tränkle C, Holzgrabe U, Höltje H-D, and Mohr K (2007) Allosteric Small Molecules Unveil a Role of an Extracellular E2/Transmembrane Helix 7 Junction for G Protein-coupled Receptor Activation. *J Biol Chem* **282**:34968–34976.

Kennedy DP, McRobb FM, Leonhardt SA, Purdy M, Figler H, Marshall MA, Chordia M, Figler RA, Linden J, Abagyan R, and Yeager M (2014) The Second Extracellular Loop of the Adenosine A_1 Receptor Mediates Activity of Allosteric Enhancers. *Mol Pharmacol* **85**:301–309.

Kruse AC, Ring AM, Manglik A, Hu J, Hu K, Eitel K, Hübner H, Pardon E, Valant C, Sexton PM,

Christopoulos A, Felder CC, Gmeiner P, Steyaert J, Weis WI, Garcia KC, Wess J, and Kobilka BK (2013) Activation and allosteric modulation of a muscarinic acetylcholine receptor. *Nature* **504**:101–106.

Leach K, Loiacono RE, Felder CC, McKinzie DL, Mogg A, Shaw DB, Sexton PM, and Christopoulos A (2010) Molecular mechanisms of action and in vivo validation of an M_4 muscarinic acetylcholine receptor allosteric modulator with potential antipsychotic properties. *Neuropsychopharmacology* **35**:855–869.

Leach K, Sexton PM, and Christopoulos A (2007) Allosteric GPCR modulators: taking advantage of permissive receptor pharmacology. *Trends Pharmacol Sci* **28**:382–389.

Lebon G, Warne T, Edwards PC, Bennett K, Langmead CJ, Leslie AGW, and Tate CG (2011) Agonist-bound adenosine A_{2A} receptor structures reveal common features of GPCR activation. *Nature* **474**:521–525.

Mackerell AD Jr., Feig M, and Brooks CL III (2004) Extending the treatment of backbone energetics in protein force fields: Limitations of gas-phase quantum mechanics in reproducing protein conformational distributions in molecular dynamics simulations. *J Comput Chem* **25**:1400–1415.

MacKerell AD, Bashford D, Bellott, Dunbrack RL, Evanseck JD, Field MJ, Fischer S, Gao J, Guo H, Ha S, Joseph-McCarthy D, Kuchnir L, Kuczera K, Lau FTK, Mattos C, Michnick S, Ngo T, Nguyen DT, Prodhom B, Reiher WE, Roux B, Schlenkrich M, Smith JC, Stote R, Straub J, Watanabe M, Wiórkiewicz-Kuczera J, Yin D, and Karplus M (1998) All-Atom Empirical Potential for Molecular Modeling and Dynamics Studies of Proteins. *J Phys Chem B* **102**:3586–3616.

May LT, and Christopoulos A (2003) Allosteric modulators of G-protein-coupled receptors. *Curr Opin Pharmacol* **3**:551–556.

May LT, Avlani VA, Langmead CJ, Herdon HJ, Wood MD, Sexton PM, and Christopoulos A (2007a) Structure-Function Studies of Allosteric Agonism at M_2 Muscarinic Acetylcholine

Receptors. *Mol Pharmacol* **72**:463–476.

May LT, Leach K, Sexton PM, and Christopoulos A (2007b) Allosteric Modulation of G Protein–Coupled Receptors. *Annu Rev Pharmacol Toxicol* **47**:1–51.

May LT, Self TJ, Briddon SJ, and Hill SJ (2010) The Effect of Allosteric Modulators on the Kinetics of Agonist-G Protein-Coupled Receptor Interactions in Single Living Cells. *Mol Pharmacol* **78**:511–523.

Narlawar R, Lane JR, Doddareddy M, Lin J, Brussee J, and IJzerman AP (2010) Hybrid ortho/allosteric ligands for the adenosine A_1 receptor. *J Med Chem* **53**:3028–3037.

Nawaratne V, Leach K, Felder CC, Sexton PM, and Christopoulos A (2010) Structural determinants of allosteric agonism and modulation at the M_4 muscarinic acetylcholine receptor: identification of ligand-specific and global activation mechanisms. *J Biol Chem* **285**:19012–19021.

Nguyen AT, Baltos J, Thomas T, Nguyen TD, López Muñoz L, Gregory KJ, White PJ, Sexton PM, Christopoulos A, and May TL (2016) Extracellular loop 2 of the adenosine A_1 receptor has a key role in orthosteric ligand affinity and agonist efficacy. *Mol Pharmacol* **In Press.**

Overington JP, Al-Lazikani B, and Hopkins AL (2006) How many drug targets are there? *Nat Rev Drug Discov* **5**:993–996.

Pan HL, Xu Z, Leung E, and Eisenach JC (2001) Allosteric adenosine modulation to reduce allodynia. *Anesthesiology* **95**:416–420.

Park SW, Kim JY, Ham A, Brown KM, Kim M, D'Agati VD, and Lee HT (2012) A_1 adenosine receptor allosteric enhancer PD-81723 protects against renal ischemia-reperfusion injury. *Am J Physiol Renal Physiol* **303**:F721–32.

Peeters MC, Wisse LE, Dinaj A, Vroling B, Vriend G, and IJzerman AP (2012) The role of the second and third extracellular loops of the adenosine A_1 receptor in activation and allosteric modulation. *Biochem Pharmacol* **84**:76–87.

Phillips JC, Braun R, Wang W, Gumbart J, Tajkhorshid E, Villa E, Chipot C, Skeel RD, Kalé L, and Schulten K (2005) Scalable molecular dynamics with NAMD. *J Comput Chem* **26**:1781–

1802.

Romagnoli R, Baraldi PG, Moorman AR, Borea PA, and Varani K (2015) Current status of A_1 adenosine receptor allosteric enhancers. *Future Med Chem* **7**:1247–1259.

Shonberg J, Herenbrink CK, López L, Christopoulos A, Scammells PJ, Capuano B, and Lane JR (2013) A structure-activity analysis of biased agonism at the dopamine D_2 receptor. *J Med Chem* **56**:9199–9221.

Valant C, Aurelio L, Devine SM, Ashton TD, White JM, Sexton PM, Christopoulos A, and Scammells PJ (2012) Synthesis and characterization of novel 2-amino-3-benzoylthiophene derivatives as biased allosteric agonists and modulators of the adenosine A(1) receptor. *J Med Chem* **55**:2367–2375.

Valant C, Aurelio L, Urmaliya VB, White P, Scammells PJ, Sexton PM, and Christopoulos A (2010) Delineating the Mode of Action of Adenosine A_1 Receptor Allosteric Modulators. *Mol Pharmacol* **78**:444–455.

Valant C, May LT, Aurelio L, Chuo CH, White PJ, Baltos J-A, Sexton PM, Scammells PJ, and Christopoulos A (2014) Separation of on-target efficacy from adverse effects through rational design of a bitopic adenosine receptor agonist. *Proc Natl Acad Sci U S A* **111**:4614–4619.

Vanommeslaeghe K, Hatcher E, Acharya C, Kundu S, Zhong S, Shim J, Darian E, Guvench O, Lopes P, Vorobyov I, and MacKerell AD (2010) CHARMM general force field: A force field for drug-like molecules compatible with the CHARMM all-atom additive biological force fields. *J Comput Chem* **31**:671–690.

Vecchio EA, Tan CY, Gregory KJ, Christopoulos A, White PJ, and May LT (2016) Ligand-independent adenosine A2B receptor constitutive activity as a promoter of prostate cancer cell proliferation. *J Pharmacol Exp Ther* **357:**36-44.

Voigtlander U, Johren K, Mohr M, Raasch A, Trankle C, Buller S, Ellis J, Holtje HD, and Mohr K (2003) Allosteric site on muscarinic acetylcholine receptors: Identification of two amino acids in the muscarinic M2 receptor that account entirely for the M2/M5 subtype selectivities of some

structurally diverse allosteric ligands in N-methylscopolamine-occupied receptors. *Mol Pharmacol* **64**:21–31.

Wootten D, Christopoulos A, and Sexton PM (2013) Emerging paradigms in GPCR allostery: implications for drug discovery. *Nat Rev Drug Discov* **12**:630–644.

Xu F, Wu H, Katritch V, Han GW, Jacobson KA, Gao ZG, Cherezov V, and Stevens RC (2011) Structure of an Agonist-Bound Human A_{2A} Adenosine Receptor. *Science* **332**:322–327.

Yu W, He X, Vanommeslaeghe K, and MacKerell AD (2012) Extension of the CHARMM General Force Field to sulfonyl-containing compounds and its utility in biomolecular simulations. *J Comput Chem* **33**:2451–2468.

Footnotes

This work was funded by the National Health and Medical Research Council of Australia (NHMRC) [Program Grant APP1055134, Project Grant APP1084487, Project Grant APP1084246]. ATNN is a recipient of an Australian Endeavour Scholarship and Fellowship. LTM is a recipient of an Australian Research Council (ARC) Discovery Early Career Researcher Award (DECRA), AC is a Senior Principal Research Fellow, and PMS is a Principal Research Fellow, of the NHMRC. KJG is a NHMRC Overseas Biomedical Postdoctoral Training Fellow.

Molecular Pharmacology Fast Forward. Published on September 28, 2016 as DOI: 10.1124/mol.116.105015
This article has not been copyedited and formatted. The final version may differ from this version.

Figure Legends

Fig. 1. Chemical structures of allosteric ligands used in the current study.

Fig. 2. Allosteric modulation of orthosteric ligand binding and function at the WT 3xHA-A_1AR. [^{3}H]DPCPX interaction binding in the presence of the orthosteric agonist NECA and PD81723 (**A**) or VCP171 (**B**) at the WT 3xHA-A_1AR. Data points represent the mean ± S.E.M of at least 3 independent experiments performed in duplicate. The inhibition of cAMP accumulation stimulated by the orthosteric agonist NECA in the presence of PD81723 (**C**) or VCP171 (**D**) at the WT 3xHA-A_1AR. Data points represent the mean ± S.E.M of at least 3 independent experiments performed in duplicate. Where error bars are not shown, they lie within the dimensions of the symbol.

Fig. 3. The change from WT (Δ WT) in affinity (pK_B; black), allosteric binding cooperativity ($log\alpha_I$; orange), allosteric functional cooperativity ($log\alpha\beta$; green) and efficacy ($log\tau_{B(C)}$; blue) of PD81723 (**A**) and VCP171 (**B**) at mutant 3xHA-A_1ARs. Data represents the mean ± S.E.M of at least 3 experiments performed in duplicate. Oversized data points are significantly different ($P<0.05$) to WT (one-way analysis of variance, Dunnett's post hoc test).

Fig. 4. Docking poses of NECA (green carbon sticks), PD81723 (magenta carbon sticks) and VCP171 (yellow carbon sticks) at the homology model of the A_1AR (grey ribbons) based on the high-resolution crystal structure of A_{2A}AR (PDB ID 3QAK). The transmembrane site is shown as a yellow surface whereas the extracellular site is shown as a red surface. Figure was generated using ICM v3.8.0.

Fig. 5. The trajectory of PD81723 (**A**) and VCP171 (**B**) during 40 ns MD simulation performed for the allosteric ligands docked into the pocket located within the extracellular vestibule bordered by TM2, ECL2, TM6, ECL3 and TM7 at the partially active A_1AR homology model (light blue

ribbons). The PD81723 and VCP171 trajectories are shown as 1 ns intervals with the beginning of the trajectory highlighted in magenta and yellow carbon sticks, respectively, and the end in white. The start and end poses are shown in thick sticks, whereas the intermediate poses are shown in thin sticks. Nitrogen, oxygen, fluorine, sulfur and polar hydrogen atoms are shown in blue, red, cyan, deep yellow and white, respectively. For the trajectory, the receptor-ligand structures were aligned by the backbone of the protein. Figures were generated using PYMOL.

Fig. 6. A_1AR residues located within 3.5 Å of PD81723 (**A**) and VCP171 (**B**) heavy atoms during the MD simulations. Values were calculated at 10 ps intervals and represent the percentage time (5% minimum threshold) for each MD simulation that the residue and ligand heavy atoms are within 3.5 Å distance.

Fig. 7. Predicted binding mode of PD81723 at the partially active A_1AR homology model. **A)** Side view of the A_1AR homology model (light blue) co-bound with NECA (green sticks) and PD81723 (magenta carbon sticks). **B)** Key residues (green sticks) bordering the PD81723 (magenta carbon sticks) binding site that were involved in hydrogen bond interactions (black dotted line) during the MD simulations. **C-F**) Residues at which alanine substitutions significantly decreased (orange sticks) or enhanced (blue sticks) PD81723 affinity (**C**), binding cooperativity (**D**), efficacy (**E**), and functional cooperativity (**F**). Figures were generated using PYMOL.

Fig. 8. Predicted binding mode of VCP171 at the partially active A_1AR homology model. **A)** Side view of the A_1AR homology model (light blue) co-bound with NECA (green sticks) and VCP171 (yellow carbon sticks). **B)** Key residue (green sticks) bordering the VCP171 (yellow carbon sticks) binding site that were involved in hydrogen bond interactions (black dotted line) during the MD simulations. **C-F**) Residues at which alanine substitutions significantly decreased (orange sticks)

Molecular Pharmacology Fast Forward. Published on September 28, 2016 as DOI: 10.1124/mol.116.105015
This article has not been copyedited and formatted. The final version may differ from this version.

VCP171 affinity (**C**), binding cooperativity (**D**), efficacy (**E**), and functional cooperativity (**F**). Figures were generated using PYMOL.

Table 1. Allosteric ligand affinity (pK_B) and binding cooperativity with NECA ($log\alpha_I$) for WT and mutant 3xHA-A_1ARs determined from whole cell [^{3}H]DPCPX binding interaction studies. Values represent the mean ± S.E.M. from indicated number of separate experiments (n) performed in duplicate.

	pK_B[a]		$log\alpha_I$[b] (α_I)		$log\alpha_I + pK_B$	
	PD81723	**VCP171**	**PD81723**	**VCP171**	**PD81723**	**VCP171**
WT	5.41 ± 0.06 (n=30)	5.65 ± 0.06 (n=10)	0.88 ± 0.05 (7.62)	0.68 ± 0.07 (4.79)	6.29	6.33
F144A	5.73 ± 0.14 (n=7)	5.48 ± 0.07 (n=3)	0.53 ± 0.15 (3.40)	0.36 ± 0.13 (2.31)	6.26	5.84
G145A	5.20 ± 0.09 (n=6)	5.32 ± 0.19 (n=3)	0.91 ± 0.11 (8.22)	0.69 ± 0.14 (4.94)	6.11	6.01
W146A	5.49 ± 0.31 (n=3)	5.65 ± 0.11 (n=3)	0.96 ± 0.27 (9.20)	0.08 ± 0.23 (1.20)*	6.45	5.73
N147A	6.15 ± 0.25 (n=3)*	5.48 ± 0.06 (n=3)	0.26 ± 0.21 (1.81)*	0.61 ± 0.07 (4.11)	6.41	6.09
N148A	5.93 ± 0.20 (n=5)*	5.72 ± 0.04 (n=3)	0.31 ± 0.08 (2.04)*	0.36 ± 0.07 (2.29)	6.24	6.08
L149A	5.77 ± 0.21 (n=5)	5.67 ± 0.03 (n=3)	0.45 ± 0.13 (2.80)	0.44 ± 0.11 (2.79)	6.22	6.11
SV150AA	5.04 ± 0.10 (n=8)	5.52 ± 0.19 (n=3)	1.16 ± 0.12 (14.35)	0.82 ± 0.1 (6.58)	6.20	6.34
E153A	5.71 ± 0.14 (n=7)	5.38 ± 0.11 (n=4)	0.58 ± 0.09 (3.76)	0.76 ± 0.19 (5.77)	6.29	6.14
R154A	5.49 ± 0.13 (n=7)	5.91 ± 0.08 (n=5)	0.75 ± 0.12 (5.57)	0.26 ± 0.12 (1.84)	6.24	6.17
W156A	5.40 ± 0.12 (n=8)	5.92 ± 0.13 (n=4)	0.95 ± 0.14 (8.87)	0.05 ± 0.05 (1.12)*	6.35	5.97
N159A	5.54 ± 0.13 (n=6)	5.93 ± 0.11 (n=6)	0.57 ± 0.1 (3.72)	0.32 ± 0.07 (2.10)	6.11	6.25

G160A	5.76 ± 0.14 (n=7)	5.96 ± 0.05 (n=3)	0.47 ± 0.11 (2.95)*	0.39 ± 0.09 (2.47)	6.23	6.35
S161A	6.18 ± 0.05 (n=5)*	5.63 ± 0.15 (n=3)	-0.32 ± 0.25 (0.47)*	0.86 ± 0.22 (7.25)	5.86	6.49
MGE162AAA	5.41 ± 0.07 (n=6)	5.61 ± 0.02 (n=3)	1.04 ± 0.16 (10.99)	0.55 ± 0.25 (3.59)	6.45	6.16
P165A	5.79 ± 0.09 (n=6)	5.95 ± 0.12 (n=4)	0.77 ± 0.09 (5.85)	0.27 ± 0.05(1.85)	6.56	6.22
V166A	5.95 ± 0.11 (n=6)*	5.80 ± 0.13 (n=6)	0.58 ± 0.09 (3.76)	0.47 ± 0.09 (2.96)	6.53	6.27
I167A	6.21 ± 0.11 (n=6)*	5.90 ± 0.15 (n=6)	0.57 ± 0.08 (3.72)	0.72 ± 0.14 (5.29)	6.78	6.62
K168A	5.86 ± 0.14 (n=7)*	5.49 ± 0.06 (n=5)	0.67 ± 0.1 (4.69)	0.68 ± 0.07 (4.84)	6.53	6.17
E170A	6.00 ± 0.11 (n=7)*	5.72 ± 0.11 (n=5)	0.46 ± 0.11 (2.89)*	0.49 ± 0.13 (3.11)	6.46	6.21
E172A	4.89 ± 0.11 (n=5)*	5.26 ± 0.05 (n=6)*	1.10 ± 0.1 (12.62)	0.84 ± 0.04 (6.93)	5.99	6.1
K173A	6.20 ± 0.11 (n=6)*	5.37 ± 0.09 (n=5)	0.32 ± 0.08 (2.08)*	0.66 ± 0.08 (4.57)	6.52	6.03
V174A	5.91 ± 0.21 (n=4)	5.91 ± 0.13 (n=4)	0.51 ± 0.18 (3.24)	0.65 ± 0.21 (4.44)	6.42	6.56
I175A	6.49 ± 0.14 (n=4)*	5.83 ± 0.13 (n=3)	0.70 ± 0.17 (5.04)	0.24 ± 0.02 (1.74)	7.19	6.07
S176A	5.78 ± 0.16 (n=6)	5.47 ± 0.12 (n=6)	0.62 ± 0.21 (4.13)	0.80 ± 0.13 (6.27)	6.40	6.27
M177A	5.73 ± 0.09 (n=5)	5.69 ± 0.15 (n=6)	0.65 ± 0.11 (4.49)	0.84 ± 0.14 (6.92)	6.38	6.53

*P < 0.05, significantly different from WT, one-way ANOVA, Dunnett's post hoc test

[a] Negative logarithm of the equilibrium dissociation constant of PD81723 and VCP171 as estimated from equation 1

[b] Logarithm of the binding cooperativity factor estimated from equation 1. Antilogarithm is shown in parentheses.

Molecular Pharmacology Fast Forward. Published on September 28, 2016 as DOI: 10.1124/mol.116.105015
This article has not been copyedited and formatted. The final version may differ from this version.

Table 2. Allosteric ligand efficacy ($\log\tau_{B(C)}$) and functional cooperativity ($\log\alpha\beta$) for WT and mutant 3xHA-A_1ARs determined from functional interaction studies in cAMP accumulation assays. Values represent the mean ± S.E.M. from indicated number of separate experiments (n) performed in duplicate.

	$\log\tau_{B(C)}$[a]		**$\log\alpha\beta$[b] ($\alpha\beta$)**	
	PD81723	**VCP171**	**PD81723**	**VCP171**
WT	-0.13 ± 0.09 (n=8)	-0.26 ± 0.09 (n=9)	0.63 ± 0.05 (4.3)	0.61 ± 0.06 (4.1)
F144A	-0.37 ± 0.08 (n=3)	-0.59 ± 0.21 (n=3)	0.65 ± 0.06 (4.4)	0.47 ± 0.08 (2.9)
G145A	-0.70 ± 0.35 (n=3)	-0.74 ± 0.09 (n=3)	0.64 ± 0.08 (4.4)	0.55 ± 0.10 (3.5)
W146A	-0.62 ± 0.27 (n=3)	-0.35 ± 0.12 (n=3)	0.57 ± 0.04 (3.7)	0.50 ± 0.05 (3.2)
N147A	-0.32 ± 0.16 (n=3)	-0.28 ± 0.17 (n=3)	0.38 ± 0.13 (2.4)	0.62 ± 0.09 (4.2)
N148A	-0.80 ± 0.21 (n=3)*	-1.24 ± 0.36 (n=3)*	0.54 ± 0.06 (3.5)	0.36 ± 0.07 (2.3)
L149A	-0.40 ± 0.2 (n=3)	-0.31 ± 0.07 (n=3)	0.33 ± 0.11 (2.1)	0.33 ± 0.05 (2.1)
SV152AA	-0.10 ± 0.20 (n=3)	-0.14 ± 0.13 (n=3)	0.84 ± 0.10 (6.9)	0.53 ± 0.05 (3.4)
E153A	-0.78 ± 0.08 (n=3)*	-1.37 ± 0.12 (n=3)*	0.67 ± 0.18 (4.7)	0.59 ± 0.09 (3.9)
R154A	-0.63 ± 0.21 (n=3)	-1.04 ± 0.18 (n=3)*	0.63 ± 0.03 (4.3)	0.26 ± 0.02 (1.8)*
W156A	-0.31 ± 0.19 (n=3)	-0.66 ± 0.18 (n=3)	0.66 ± 0.05 (4.5)	0.29 ± 0.06 (2.0)*
N159A	-0.56 ± 0.14 (n=3)	-0.72 ± 0.04 (n=3)	0.44 ± 0.08 (2.8)	0.25 ± 0.04 (1.8)*
G160A	-0.43 ± 0.09 (n=3)	-0.46 ± 0.16 (n=3)	0.58 ± 0.07 (3.8)	0.51 ± 0.04 (3.2)
S161A	-0.85 ± 0.29 (n=3)*	-1.21 ± 0.59 (n=3)*	0.32 ± 0.06 (2.1)	0.33 ± 0.03 (2.1)
MGE162AAA	-0.43 ± 0.30 (n=3)	-0.15 ± 0.13 (n=3)	0.55 ± 0.19 (3.5)	0.49 ± 0.17 (3.1)
P165A	-0.07 ± 0.08 (n=4)	-0.28 ± 0.01 (n=3)	0.59 ± 0.05 (3.9)	0.46 ± 0.07 (2.9)
V166A	-0.27 ± 0.09 (n=4)	-0.40 ± 0.13 (n=3)	0.59 ± 0.04 (3.9)	0.42 ± 0.08 (2.6)
I167A	-0.78 ± 0.17 (n=4)*	-1.07 ± 0.30 (n=3)*	0.49 ± 0.08 (3.1)	0.38 ± 0.01 (2.4)
K168A	-0.11 ± 0.05 (n=4)	-0.29 ± 0.12 (n=3)	0.49 ± 0.07 (3.1)	0.48 ± 0.14 (3.0)
E170A	-0.43 ± 0.13 (n=4)	-0.60 ± 0.14 (n=3)	0.51 ± 0.07 (3.3)	0.42 ± 0.12 (2.6)

Molecular Pharmacology Fast Forward. Published on September 28, 2016 as DOI: 10.1124/mol.116.105015
This article has not been copyedited and formatted. The final version may differ from this version.

E172A	-0.39 ± 0.29 (n=3)	-0.63 ± 0.04 (n=3)	0.95±0.18 (8.9)*	0.62 ± 0.04 (4.2)
K173A	-0.60 ± 0.21 (n=3)	-0.53 ± 0.27 (n=3)	0.33 ± 0.08 (2.1)	0.38 ± 0.13 (2.4)
V174A	-0.43 ± 0.04 (n=4)	-0.66 ± 0.29 (n=3)	0.53 ± 0.04 (3.4)	0.27 ± 0.07 (1.8)*
I175A	-0.74 ± 0.06 (n=3)	-1.42 ± 0.37 (n=3)*	0.33 ± 0.10 (2.1)	0.24 ± 0.02 (1.7)*
S176A	-0.36 ± 0.11 (n=4)	-0.31 ± 0.14 (n=3)	0.57 ± 0.03 (3.7)	0.31 ± 0.07 (2.0)
M177A	-0.52 ± 0.08 (n=4)	-0.23 ± 0.08 (n=3)	0.58 ± 0.03 (3.8)	0.44 ± 0.07 (2.8)

[a] Logarithm of the efficacy parameter determined from the operational model of allosterism corrected for changes in receptor expression.

[b] Logarithm of the functional cooperativity between the allosteric ligand and NECA. Antilogarithm is shown in parentheses.

*P < 0.05, significantly different from WT, one-way ANOVA, Dunnett's post hoc test.

Fig. 1

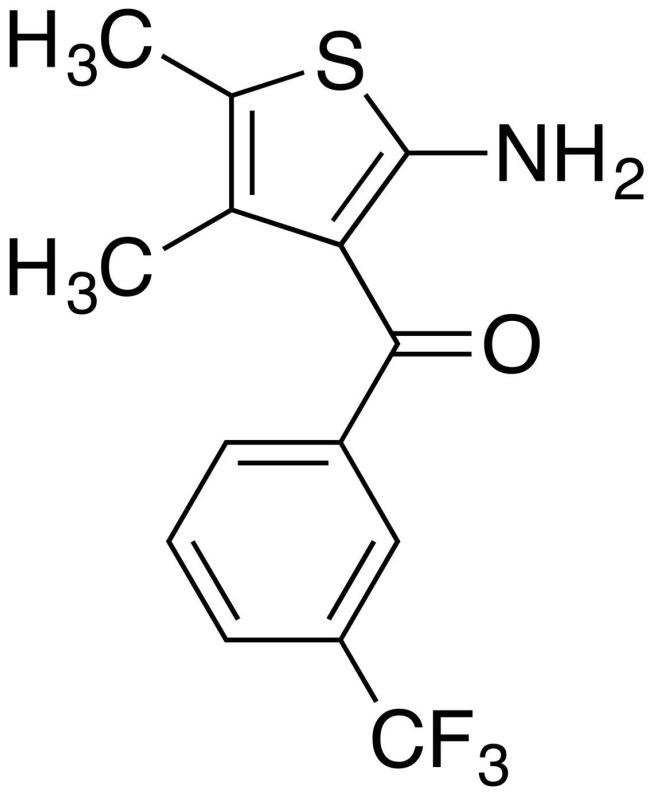

PD81723

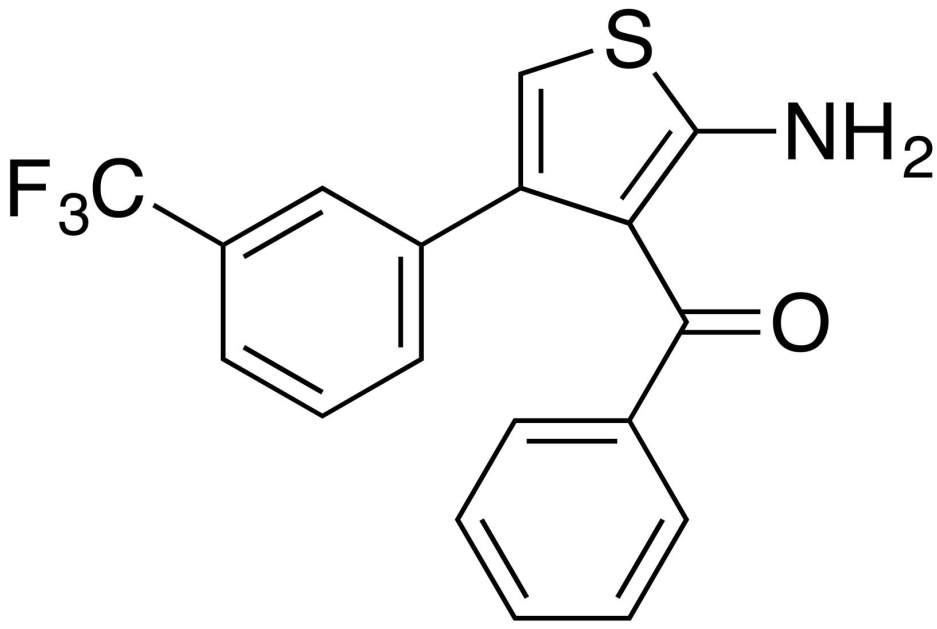

VCP171

Fig. 2

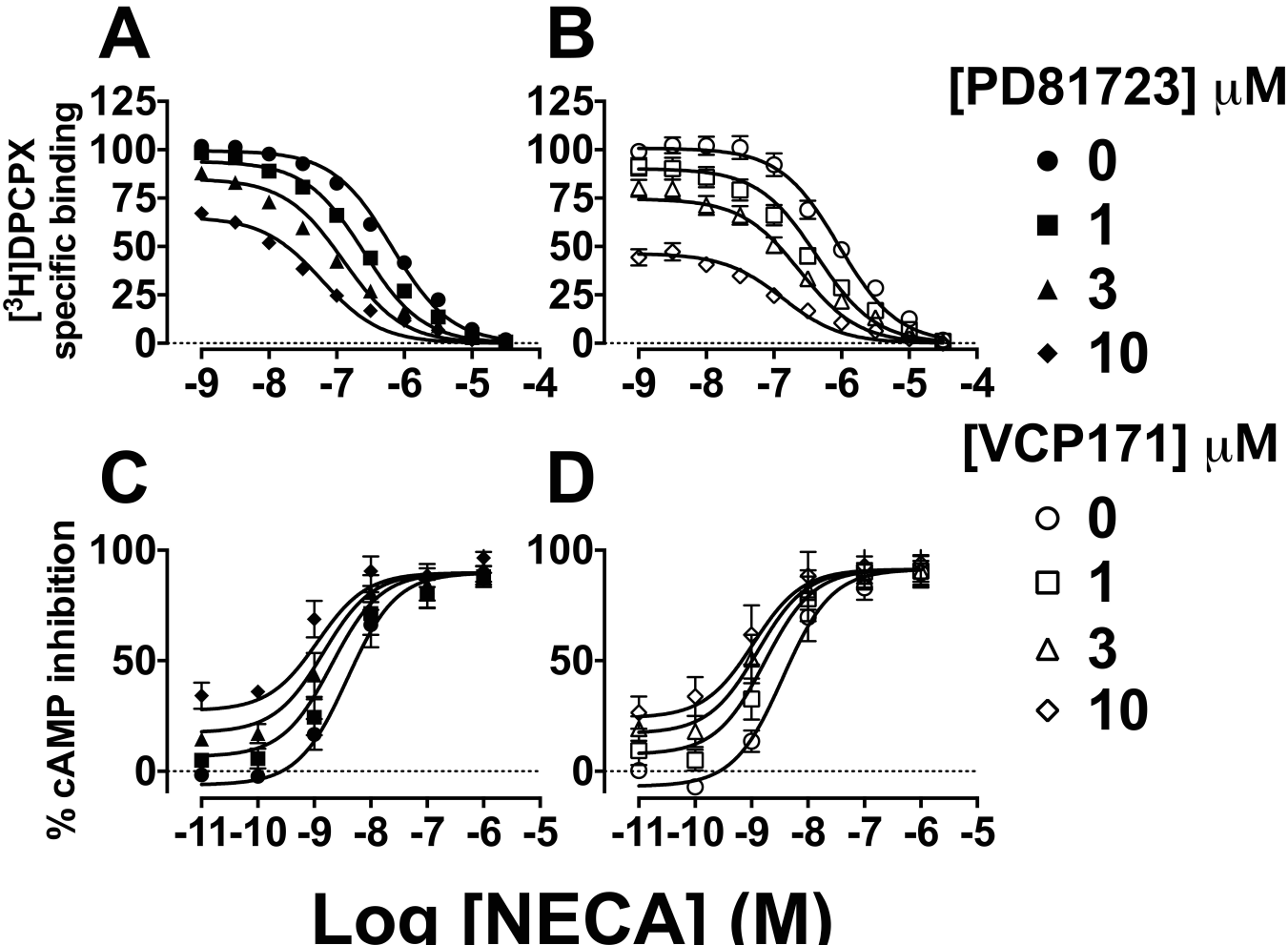
A
B
C
D
[3H]DPCPX specific binding
% cAMP inhibition
Log [NECA] (M)
[PD81723] μM
0
1
3
10
[VCP171] μM
0
1
3
10

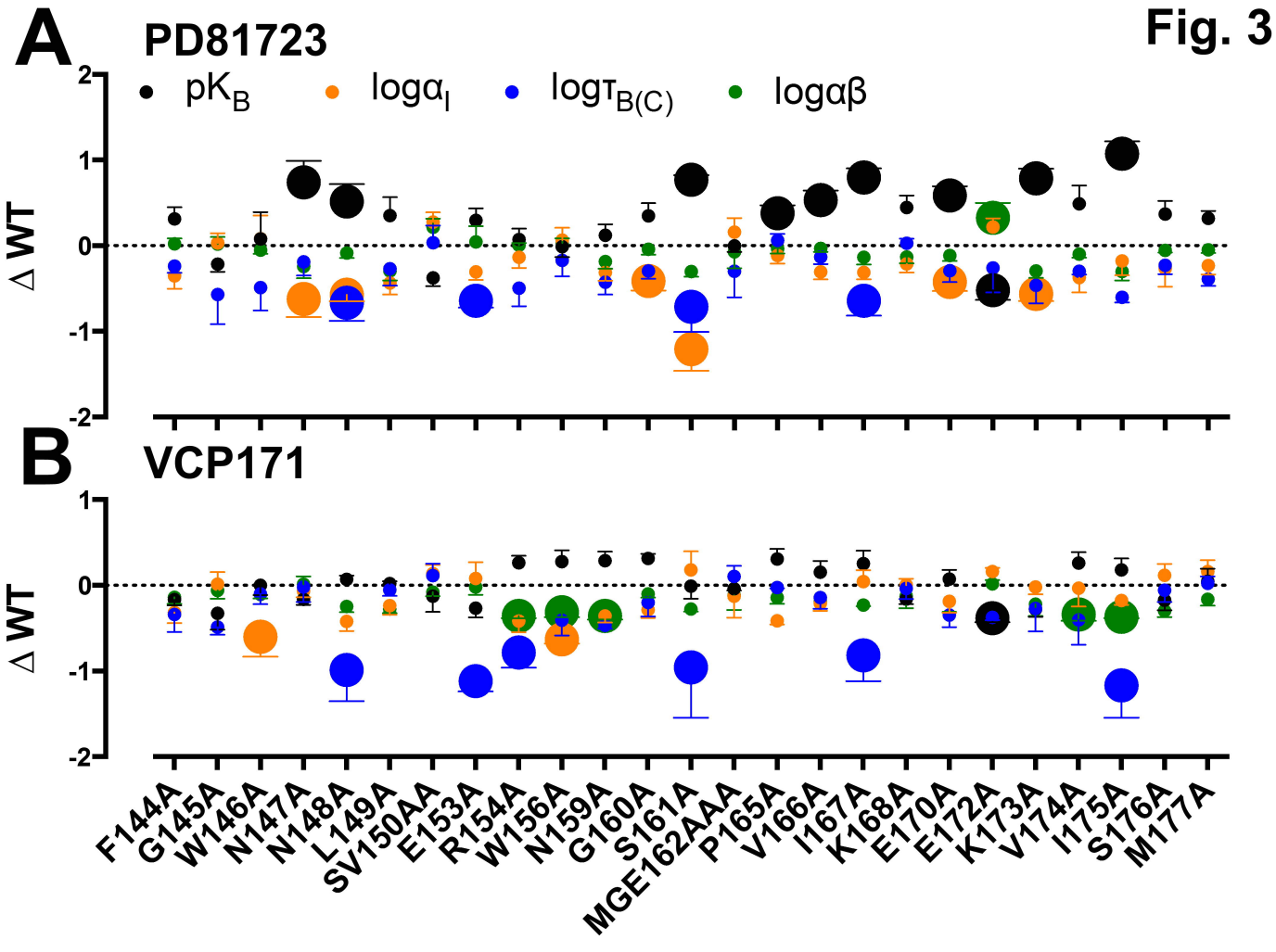
A
PD81723
pK_B
logα_I
logτ_B(C)
logαβ
Δ WT
2
1
0
-1
-2
B
VCP171
Δ WT
1
0
-1
-2
F144A
G145A
W146A
N147A
N148A
L149A
SV150AA
E153A
R154A
W156A
N159A
G160A
S161A
MGE162AAA
P165A
V166A
I167A
K168A
E170A
E172A
K173A
V174A
I175A
S176A
M177A

Fig. 4

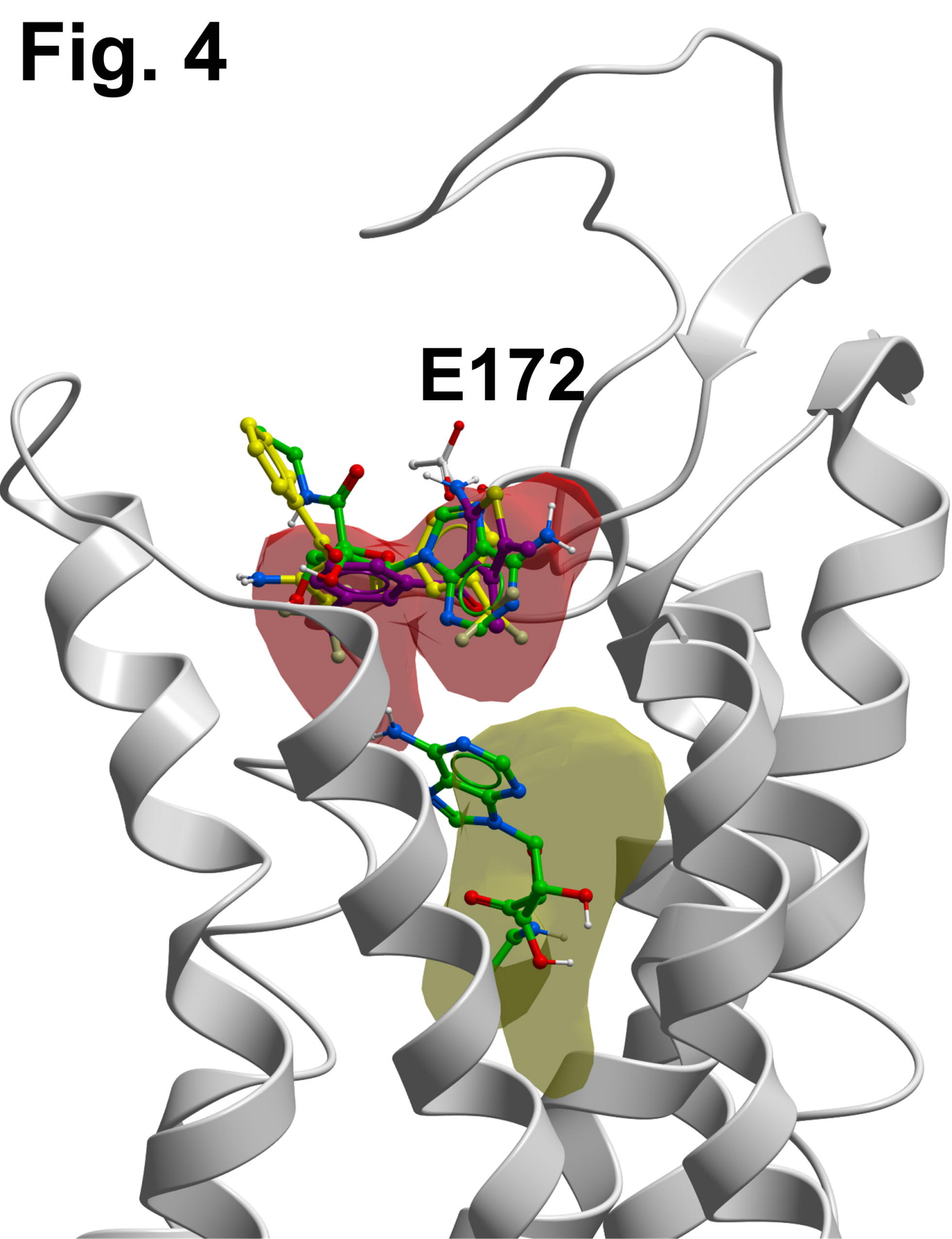

Fig. 5

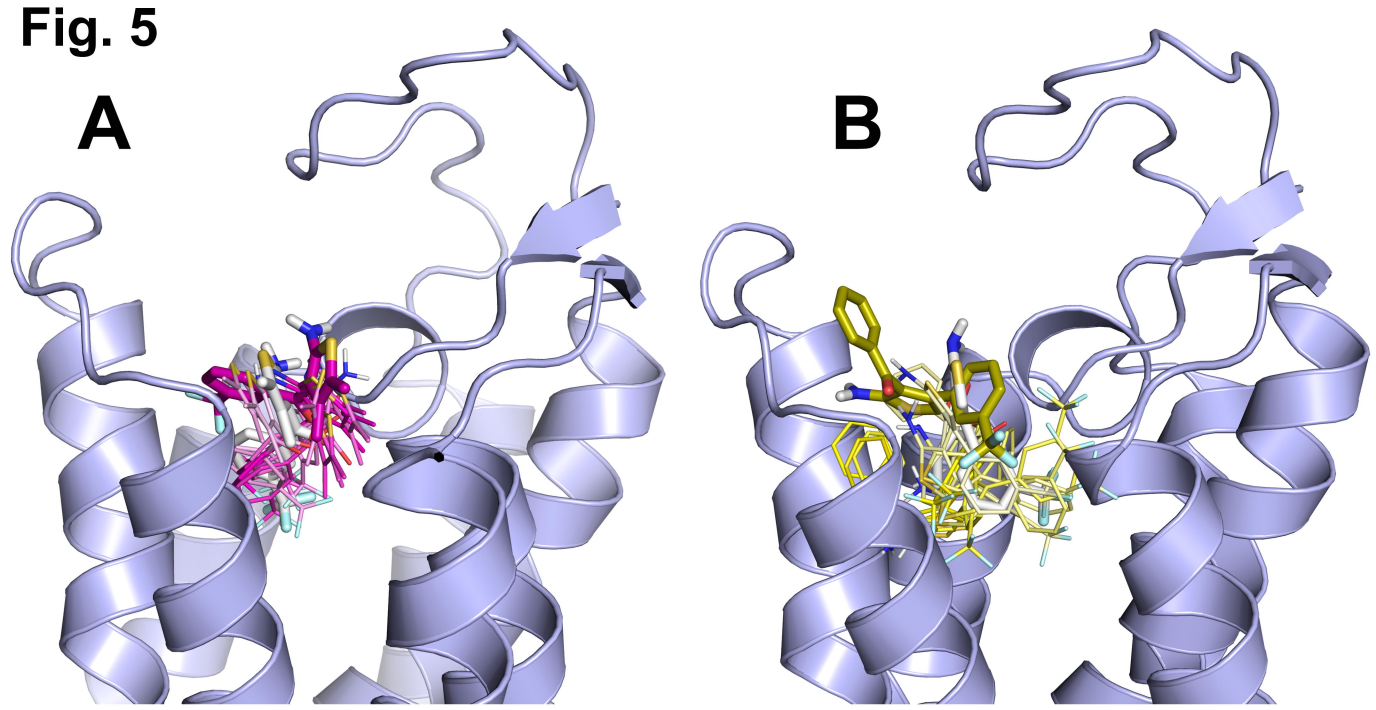

Fig. 6

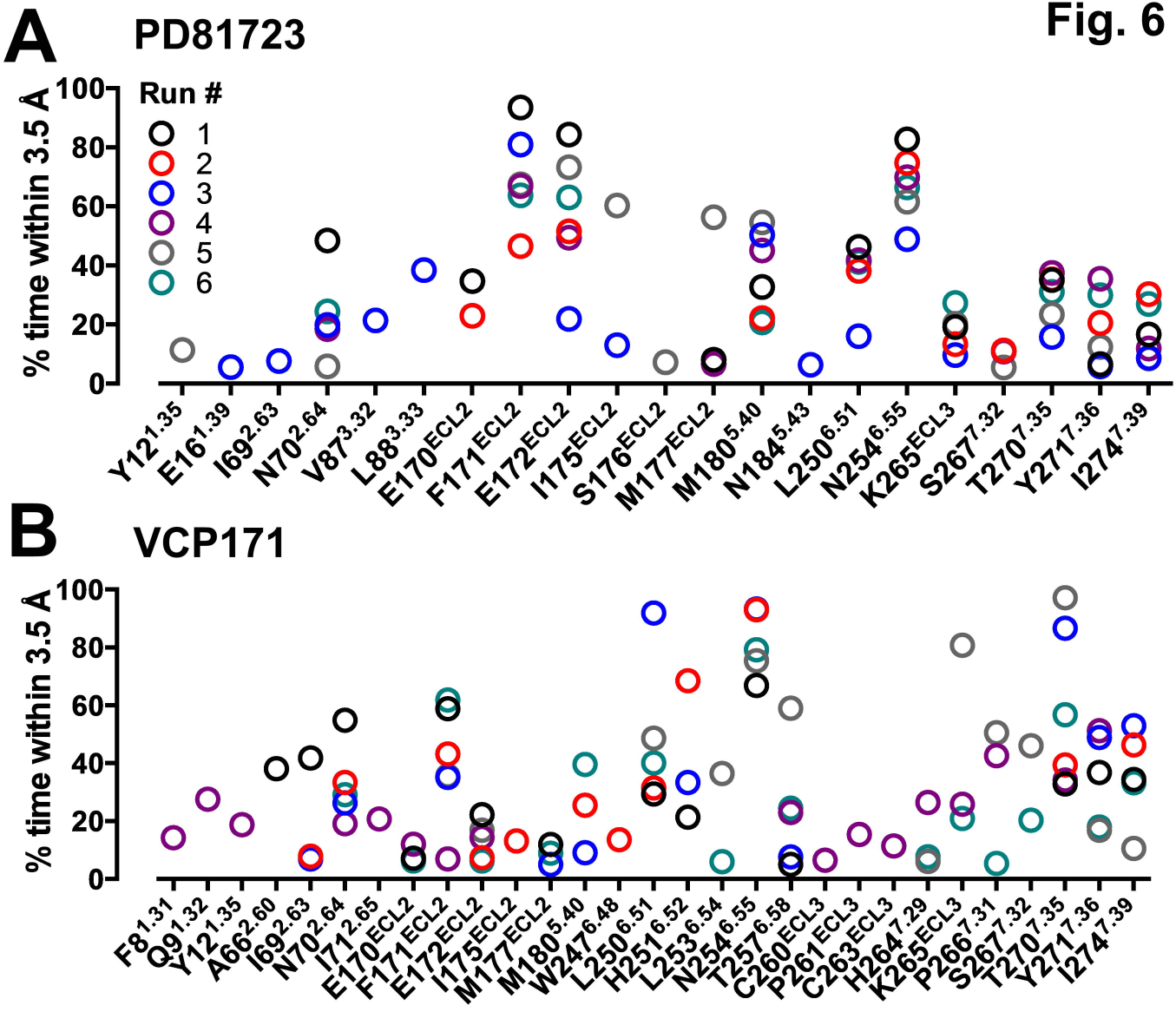
A
PD81723
% time within 3.5 Å
Run #
1
2
3
4
5
6
Y121.35
E161.39
I692.63
N702.64
V873.32
L883.33
E170ECL2
F171ECL2
E172ECL2
I175ECL2
S176ECL2
M177ECL2
M1805.40
N1845.43
L2506.51
N2546.55
K265ECL3
S2677.32
T2707.35
Y2717.36
I2747.39
B
VCP171
% time within 3.5 Å
F81.31
Q91.32
Y121.35
A662.60
I692.63
N702.64
I712.65
E170ECL2
F171ECL2
E172ECL2
I175ECL2
M177ECL2
M1805.40
W2476.48
L2506.51
H2516.52
L2536.54
N2546.55
T2576.58
C260ECL3
P261ECL3
C263ECL3
H2647.29
K265ECL3
P2667.31
S2677.32
T2707.35
Y2717.36
I2747.39

Fig. 7

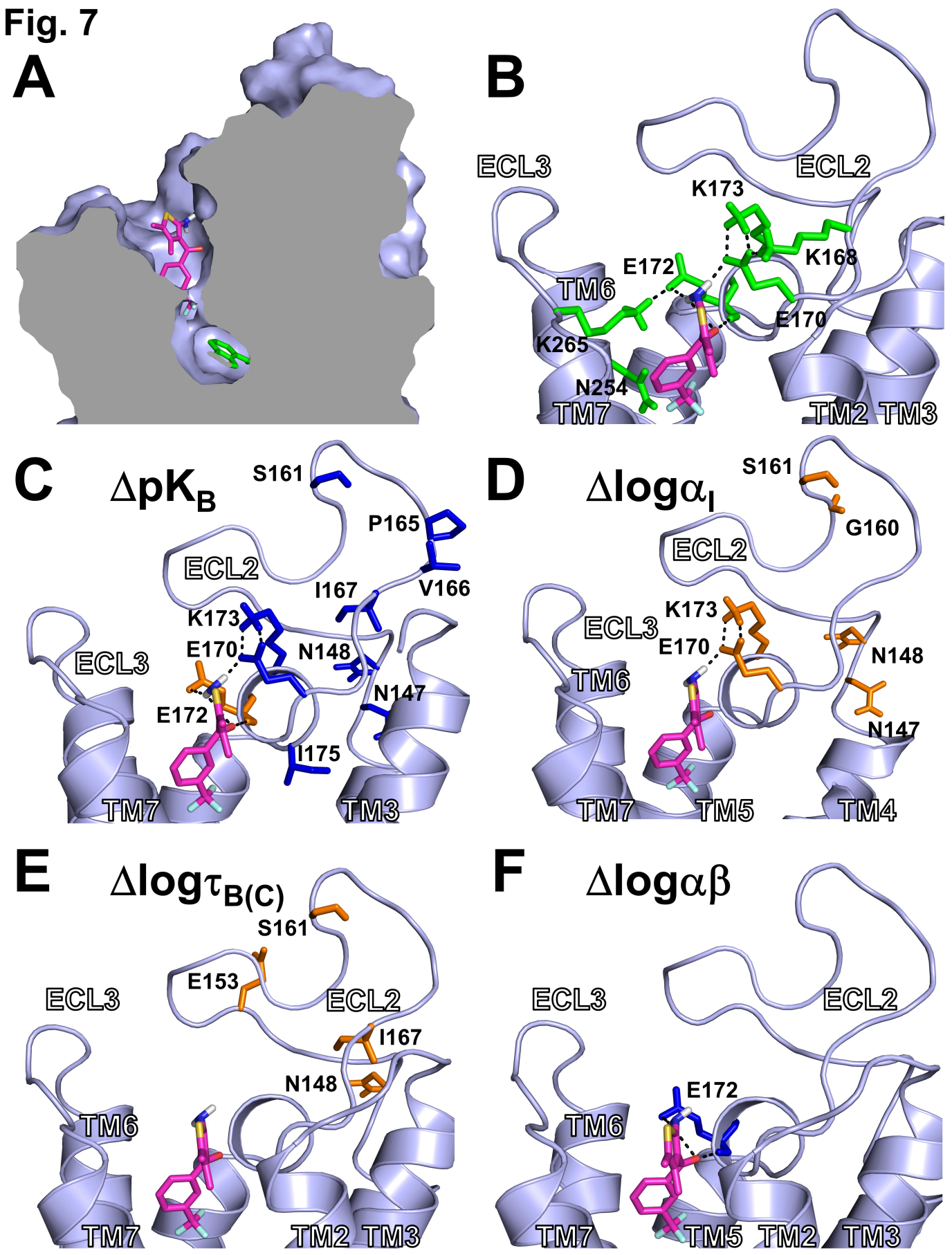
A
B
ECL3
ECL2
K173
K168
E172
TM6
E170
K265
N254
TM7
TM2
TM3
C
ΔpK_B
S161
P165
ECL2
I167
V166
K173
E170
N148
ECL3
N147
E172
I175
TM7
TM3
D
Δlogα_I
S161
G160
ECL2
K173
ECL3
E170
N148
TM6
N147
TM7
TM5
TM4
E
Δlogτ_B(C)
S161
E153
ECL3
ECL2
I167
N148
TM6
TM7
TM2
TM3
F
Δlogαβ
ECL3
ECL2
E172
TM6
TM7
TM5
TM2
TM3

Fig. 8

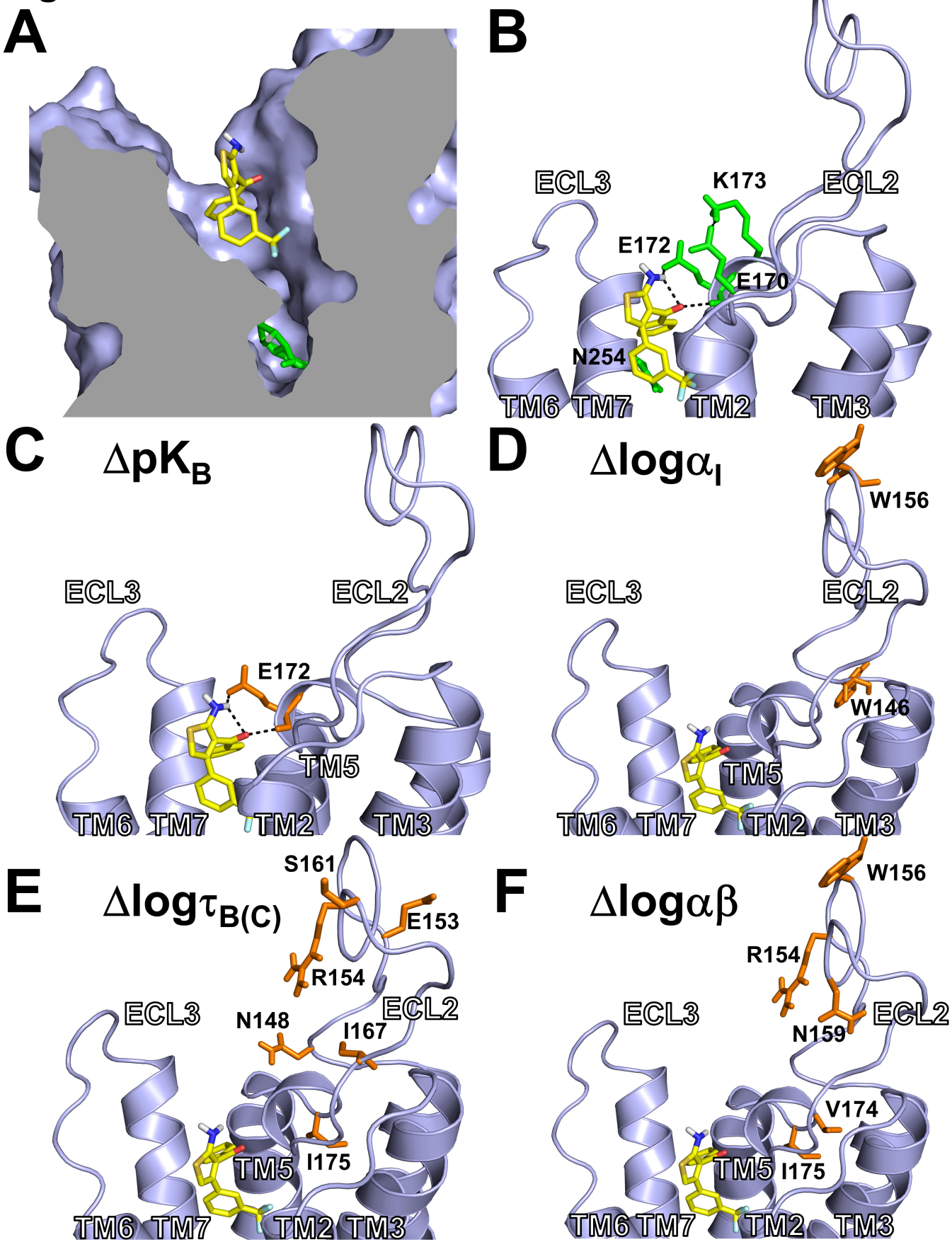
A
B
ECL3
K173
ECL2
E172
E170
N254
TM6
TM7
TM2
TM3
C
ΔpK_B
ECL3
ECL2
E172
TM5
TM6
TM7
TM2
TM3
D
Δlogα_I
W156
ECL3
ECL2
W146
TM5
TM6
TM7
TM2
TM3
E
Δlogτ_B(C)
S161
E153
R154
ECL3
N148
I167
ECL2
TM5
I175
TM6
TM7
TM2
TM3
F
Δlogαβ
W156
R154
ECL3
N159
ECL2
V174
TM5
I175
TM6
TM7
TM2
TM3